Phase Behavior of a Binary Mixture of a Block Copolymer with Lower Disorder-to-Order Transition and a Homopolymer

Eun Young Kim, Dong Jun Lee, and Jin Kon Kim*

National Creative Research Initiative Center for Block Copolymer Self-Assembly, Department of Chemical Engineering and Polymer Research Institute, Pohang University of Science & Technology, Kyungbuk 790-784, Korea

Junhan Cho*

Department of Polymer Science and Engineering, Dankook University, Hyperstructured Organic Materials Research Center, Seoul 140-714, Korea

Received August 3, 2006; Revised Manuscript Received October 2, 2006

ABSTRACT: The phase diagrams for a binary mixture of symmetric polystyrene-*block*-poly(*n*-butyl methacrylate) copolymer (PS-*b*-PnBMA) exhibiting lower disorder-to-order transition (LDOT) and PS homopolymer and a binary mixture of PS-*b*-PnBMA and PnBMA homopolymer were investigated by using polarizing optical microscopy, turbidity measurement, small-angle X-ray scattering, rheology, and transmission electron microscopy. Emphasis was placed on the effect of the molecular weight of homopolymers on the phase behavior of the mixtures. We found that when the molecular weight of a homopolymer was smaller than the half of molecular weight of the corresponding block, LDOT of the mixture increased (thus miscibility was enhanced). However, the changes of microdomains for the mixtures containing PS homopolymer are different from those for the mixtures containing PnBMA homopolymer, especially when the molecular weight of homopolymer becomes large. For instance, for the mixture of PS-*b*-PnBMA and PnBMA with a molecular weight of 65000, lamellar microdomains structure was destroyed even at the addition of 20 wt % of PnBMA homopolymer. On the other hand, for the mixture of PS-*b*-PnBMA and PS with a molecular weight 68000, the lamellar microdomain structure was maintained up to 40% of PS homopolymer. The phase diagrams of the mixtures were compared with predictions developed based on the compressible random phase approximation.

1. Introduction

The phase behavior of a binary mixture consisting of a block copolymer and a homopolymer has been extensively studied experimentally[1−26] and theoretically.[27−32] The most important parameter in determining phase behavior of the mixtures is the molecular weight ratio of a homopolymer to the corresponding block component in a block copolymer. For small molecular weights of homopolymers, these are easily dissolved in the microphase-separated structure of block copolymer. When the molecular weight of a homopolymer is much greater than that of the corresponding block, macrophase separation occurs.

All the block copolymers employed in the literature[1−26] to investigate the phase behavior of binary mixtures exhibit the order-to-disordered transition (ODT); thus, a homogeneous state of the mixture could be obtained upon heating. However, some block copolymers exhibit lower disorder-to-order transition (LDOT) upon heating.[33−39] The driving force for the LDOT is of entropic origin,[40] thus driven either by disparity in compressibility or by directional interactions, which is quite different from that for the ODT. However, to the best of our knowledge, the phase diagram of a binary mixture of a block copolymer with LDOT and a homopolymer has not been studied experimentally or theoretically.

In this paper, we first present experimentally determined phase diagrams of a binary mixture of polystyrene-*block*-poly(*n*-butyl methacrylate) copolymer (PS-*b*-PnBMA) and PS homopolymer as well as a binary mixture of PS-*b*-PnBMA and PnBMA homopolymer by using polarized optical microscopy (POM), turbidity measurement, small-angle X-ray scattering (SAXS) and transmission electron microscopy (TEM). It is noted that PS-*b*-PnBMA exhibited LDOT phase behavior.[33−35,37−39] The emphasis is placed upon the effect of the molecular weight of homopolymers on phase behavior of binary mixtures. Then, the phase diagrams of the mixtures are compared with predictions developed based on the compressible mean field theory developed by one of us.[41−45]

* To whom correspondence should be addressed. E-mail: (J.K.K.) jkkim@postech.ac.kr; (J.H.C.) jhcho@dku.edu.

2. Experimental Section

2.1. Materials and Sample Preparation. PS-*b*-PnBMA having a number-average molecular weight (M_n) of 67000 g/mol and a polydispersity index (M_w/M_n in which M_w is the weight-average molecular weight) of 1.04 was synthesized by the sequential anionic polymerization of styrene and *n*-butyl methacrylate in tetrahydrofuran containing dried LiCl at −78 °C under purified Ar using a *sec*-BuLi initiator.[39] The volume fraction of PS block in PS-*b*-PnBMA was 0.5, determined from ^{1}H nuclear magnetic resonance spectroscopy. PS and PnBMA homopolymers with various molecular weights were purchased from Aldrich Chemical Co. The molecular characteristics of PS-*b*-PnBMA and PS and PnBMA homopolymers employed in this study are given in Table 1. Various compositions of binary mixtures consisting of PS-*b*-PnBMA and PS homopolymers as well as consisting of PS-*b*-PnBMA and PnBMA homopolymers were prepared by dissolving a predetermined amount of the mixtures in toluene (10 wt % in solute) and slowly evaporating solvent over 2 weeks at room temperature. Each specimen was annealed at 120 °C for 48 h.

2.2. Polarized Optical Microscopy. A polarized optical microscope (POM; Zeiss Co.) with CCD camera was used to find whether a sample at a given temperature was in an ordered state. When a specimen is in an ordered state having lamellar or cylindrical

10.1021/ma0617567 CCC: $33.50
Published on Web 11/17/2006

Table 1. Molecular Characteristics of the Polymers Used in This Study

symbol	description	M_n	M_w
PS-*b*-PnBMA	polystyrene-*b*-poly(*n*-butyl methacrylate) copolymer	67 000	69 000
PS-2	PS homopolymer	2000	2100
PS-13	PS homopolymer	12 600	13 100
PS-20	PS homopolymer	20 000	20 800
PS-68	PS homopolymer	68 000	71 000
PnBMA-11	PnBMA homopolymer	10 500	12 700
PnBMA-24	PnBMA homopolymer	23 500	25 000
PnBMA-65	PnBMA homopolymer	65 000	68 000

microdomains, it shows distinct birefringence in the POM image, whereas no birefringence is observed in a disordered sample.[46] Since the absence of birefringence could also be observed for ordered structures with spherical or double gyroid microdomains, TEM and SAXS experiments were carried out additionally. The sample for POM was prepared by solution-casting (10 wt % in toluene) onto a cover glass and annealed at 120 °C for 4 h under a nitrogen environment to remove residual solvent.

2.3. Turbidity Experiment. Various compositions of the mixtures for the turbidity temperature (T_b) measurements were prepared by dissolving a predetermined amount of the mixtures in toluene (10 wt % in solute) and slowly evaporating solvent over 8 h at room temperature. Sample thickness was ~10 μm. Each specimen was annealed at 120 °C for 4 h. The T_b of each blend was determined by optical microscopy (OM, Axioplan, Zeiss Co.) using a heating block blanketed in nitrogen. The T_b of a specimen was estimated by the threshold temperature above which phase-separated structures were clearly seen under the OM at a heating rate of 1.5 °C/h.

2.4. Small-Angle X-ray Scattering (SAXS). SAXS profiles ($I(q)$ vs $q(=4\pi \sin\theta/\lambda)$, in which q is the scattering vector and 2θ is the scattering angle) were obtained at the 4C1 and 4C2 beamlines at the Pohang Light Source (PLS), Korea.[47] A 2-D CCD camera (Princeton Instruments Ins., SCX-TE/CCD-1242) was used to collect the scattered X-rays. The sample thickness was 1 mm and sample-to-detector distance was 2.4 m. The exposure time was 10 min.

2.5. Rheological Experiment. Temperature sweep of storage and loss moduli (G′ and G″) was performed under isochronal condition upon heating at a rate of 0.5 °C/min with an Advanced Rheometrics Expansion System (ARES) with parallel plate of 25 mm diameter. Before the experiment, the thermal history of the samples was completely removed by annealing the sample at homogeneous state of 120 °C for 4 h. The strain amplitude and the angular frequency were 0.05 and 0.1 rad/s, respectively, which lie in linear viscoelasticity.

2.6. Transmission Electron Microscopy. The microdomain structures of the mixtures were investigated with a transmission electron microscope (TEM; Hitachi-7600) operating at 80 kV. Microtoming was performed with an RMC (MT-7000) microtomer with a diamond knife at room temperature after epoxy embedding. The specimens were stained with ruthenium tetroxide (RuO_4) for 20 min at room temperature, which selectively stained the PS microdomain.

3. Results and Discussion

Figure 1 shows temporal changes of G′ and G″ of neat PS-*b*-PnBMA. G′ and G″ show rapid increase near 160 °C, which is referred to as a disorder-to-order transition (LDOT) temperature. It is known that G′ precipitously decreases at an ODT temperature upon heating for block copolymers with lamellar or cylindrical microdomains.[48−50] Insets in Figure 1 are POM images for neat PS-*b*-PnBMA at 160 and 161 °C, from which the birefringence was first detected at 161 °C.

Figure 2a shows SAXS profiles ($I(q)$ vs q) at various temperatures for neat PS-*b*-PnBMA. Even though a synchrotron source of X-ray with a relatively longer exposure time (10 min) was used, we could not find higher-order peaks, because of the small electron density difference between PS and PnBMA blocks. With increasing temperature, both $I(q)$ and the domain spacing ($D = 2\pi/q^*$, in which q^* is the maximum peak position) increased steadily. This indicates that the segregation power between two blocks increases with increasing temperature, which results from the characteristic of the LDOT type phase behavior. Parts b and c of Figure 2 give plots of $1/I(q^*)$ and D vs $1/T$, respectively, from which LDOT of neat PS-*b*-PnBMA is determined to be 162 °C. From the results given in Figures 1 and 2, LDOT determined by POM is in good agreement with that determined by SAXS and rheology. Hereafter, the LDOT of the mixtures of PS-*b*-PnBMA and homopolymers is mainly determined by POM, as long as a mixture exhibits either lamellar or cylindrical microdomain.

Figure 3 gives POM images of 80/20 (w/w) PS-*b*-PnBMA/PS-13 mixture (a and b) and 80/20 (w/w) PS-*b*-PnBMA/PS-68 mixture (c and d) at two different temperatures, from which the LDOT for these two mixtures are determined to be 216 and 152 °C, respectively. Figure 4 gives phase diagrams of the mixtures of PS-*b*-PnBMA/PS with four different molecular weights (PS-2, PS-13, PS-20, and PS-68). Here, M and H represent microphase separated and homogeneous state, respectively. L is the macrophase-separated homopolymer. The boundary between M and H (thus, LDOT), given in closed rectangles, was determined by using POM and SAXS. The macrophase-separated state (M + L) was determined by cloud point measurement, and shown as closed circles. It is seen in Figure 4 that at smaller molecular weight of PS homopolymer (PS-2) which is much smaller than that of PS block in PS-*b*-PnBMA, LDOT increased rapidly with increasing amount of PS homopolymer; thus the miscibility was greatly enhanced. For instance, the LDOT increased more than 40 °C with the addition of 10 wt % of PS-2. With increasing molecular weight, the M region becomes expanded, but at higher temperatures the macrophase-separation was observed for almost all composi-

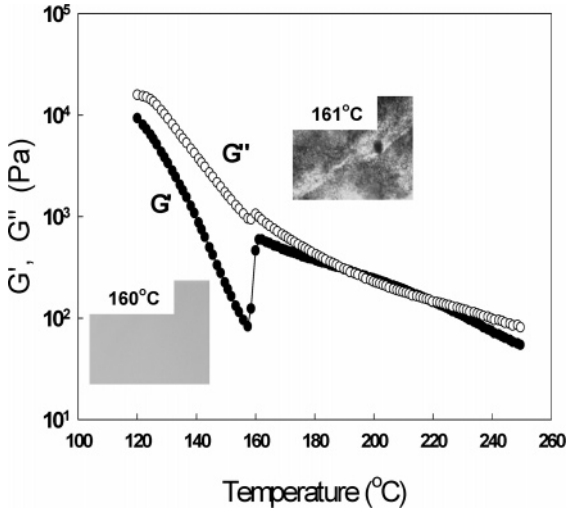

Figure 1. Temperature sweeps of G′ and G″ of neat PS-*b*-PnBMA. Insets are POM images at two temperatures (160 and 161 °C).

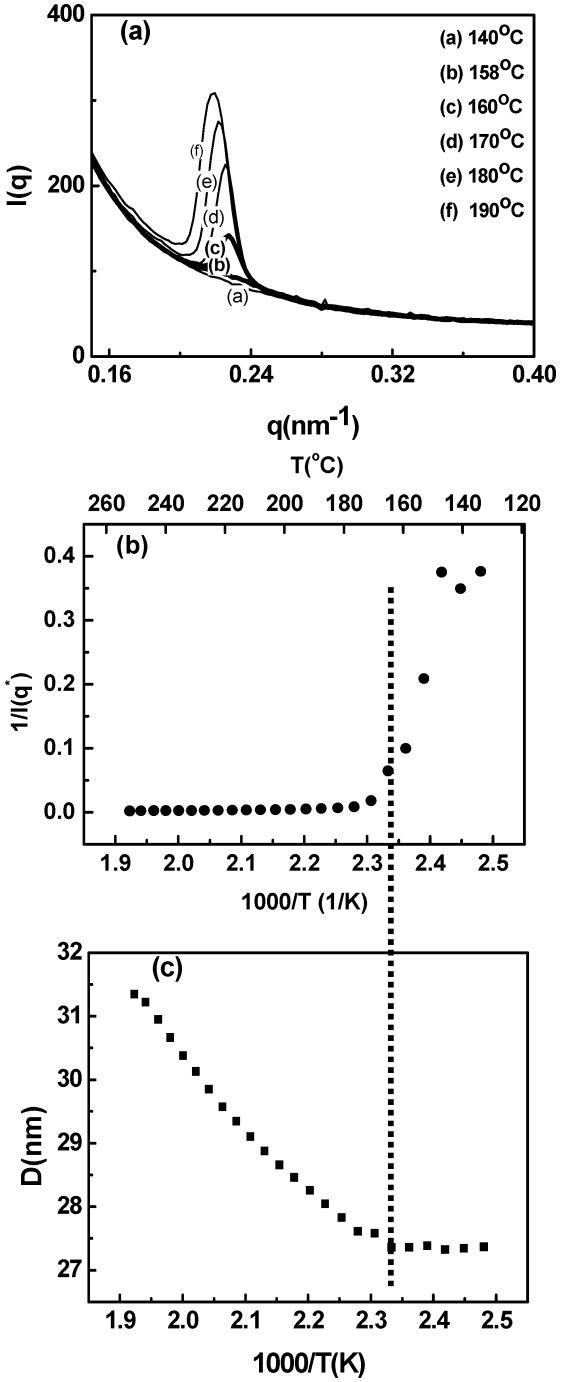

Figure 2. (a) SAXS profiles ($I(q)$ vs q) at various temperatures for neat PS-*b*-PnBMA. Plots of (b) $1/I(q^*)$ and (c) the domain size (D) vs $1/T$.

tions. At a higher molecular weight of PS (PS-68), with increasing temperature, LDOT decreased slightly at smaller amounts, but it increased again with increasing amounts of PS-68. In this situation, the macrophase separated regions were extended even at lower temperatures.

Figure 5 gives phase diagrams of the mixtures of PS-*b*-PnBMA/PnBMA with three different molecular weights (PnBMA-11, PnBMA-24, and PnBMA-65). Overall phase behaviors of these mixtures are similar to those for mixtures of PS-*b*-PnBMA/PS. However, the M region for mixture of a PS-*b*-PnBMA/PnBMA-11 is slightly expanded compared with mixture of the PS-*b*-PnBMA/PS-13, even though the molecular weight of PnBMA-11 is slightly less than that of PS-13.

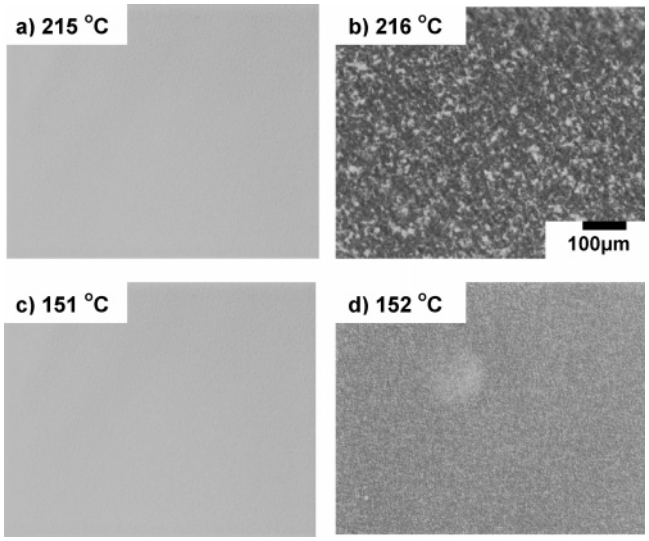

Figure 3. POM images of 80/20 (w/w) PS-*b*-PnBMA/PS-13 mixture (a and b) and 80/20 (w/w) PS-*b*-PnBMA/PS-68 mixture (c and d) at two different temperatures.

The microdomains of mixtures change greatly with the addition of high molecular weight homopolymer.[5−8] Thus, we investigated in detail the phase behavior of the mixture of PS-*b*-PnBMA/PS-68 by using SAXS and TEM. Figure 6 shows SAXS profiles at various temperatures for 60/40 (w/w) PS-*b*-PnBMA/PS-68 mixture. With increasing temperature, SAXS intensity was first detected near 168 °C (see the inset). This corresponds to the LDOT of this composition, and this is in good agreement with the result determined from POM. With increasing temperature up to 220 °C, $I(q^*)$ increases steadily. D of this mixture was ~ 41 nm, which is larger than that of neat PS-*b*-PnBMA. Figure 7 gives TEM images for various compositions of PS-*b*-PnBMA/PS-20 and PS-*b*-PnBMA/PnBMA-24 mixtures annealed at 190 °C for 5 days followed by quenching to room temperature. Neat PS-*b*-PnBMA exhibited lamellar microdomains with domain spacing of 28 nm in Figure 7a, which is consistent with SAXS measurement (see Figure 2c). The lamellar microdomains were maintained up to the weight fraction of PS-20 (w_{PS}) of 0.2 (in which the total PS weight fraction (PS block and PS-20 homopolymer) in the mixture is 0.6). As w_{PS} increased further (for instance, 60/40 (w/w) PS-*b*-PnBMA/PS-20), a disordered state (homogeneous phase) was observed at 190 °C. On the other hand, the change of microdomains with weight fraction of PnBMA homopolymer for the mixture of PS-*b*-PnBMA and PnBMA-24 at 190 °C was different from that of the mixture of PS-*b*-PnBMA and PS-20. With increasing the weight fraction of PnBMA-24 homopolymer, microdomains of the mixture of PS-*b*-PnBMA/PnBMA-24 were transformed from lamellae (Figure 7d for 80/20 (w/w) PS-*b*-PnBMA/PnBMA-24) to hexagonally packed cylinders (Figure 7e for 60/40 (w/w) PS-*b*-PnBMA/PnBMA-24) and finally to a disordered state with concentration fluctuation[51] (Figure 7f for 40/60 (w/w) PS-*b*-PnBMA/PnBMA-24). It is noted that Figure 7e does not correspond to spherical microdomains because distinct birefringence was detected.

Figure 8 gives TEM images for various compositions of PS-*b*-PnBMA/PS-68 and PS-*b*-PnBMA/PnBMA-65 mixtures annealed at 190 °C for 5 days followed by quenching to room temperature. The lamellar microdomains were maintained up to the weight fraction of PS-68 (w_{PS}) of 0.4 (in which the total PS weight fraction (PS block and PS-68 homopolymer) in this mixture was 0.7), and the D increased steadily with increasing w_{PS}. On the other hand, the change of microdomains with weight

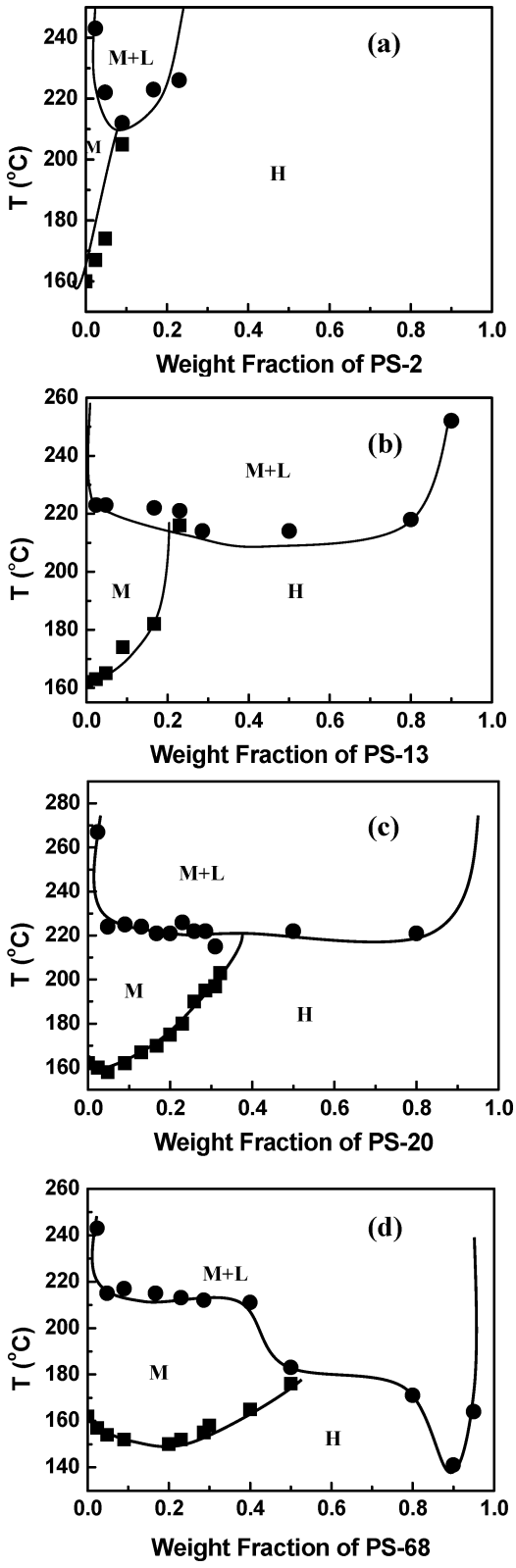

Figure 4. Phase diagrams of mixtures of PS-*b*-PnBMA/PS with four different molecular weights: (a) PS-2; (b) PS-13; (c) PS-20; (d) PS-68. Here, M, H, and L represent microphase separation, homogeneous state, and macrophase-separated PS homopolymer, respectively.

fraction of PnBMA homopolymer for the mixture of PS-*b*-PnBMA and PnBMA-65 at 190 °C was distinctly different from that of the mixture of PS-*b*-PnBMA and PS-68. Both 80/20 and 60/40 (w/w) PS-*b*-PnBMA/PnBMA-65 exhibited ill-defined microdomains not belonging to lamellae or cylinders. But, a distinct birefringence was detected for both compositions. The

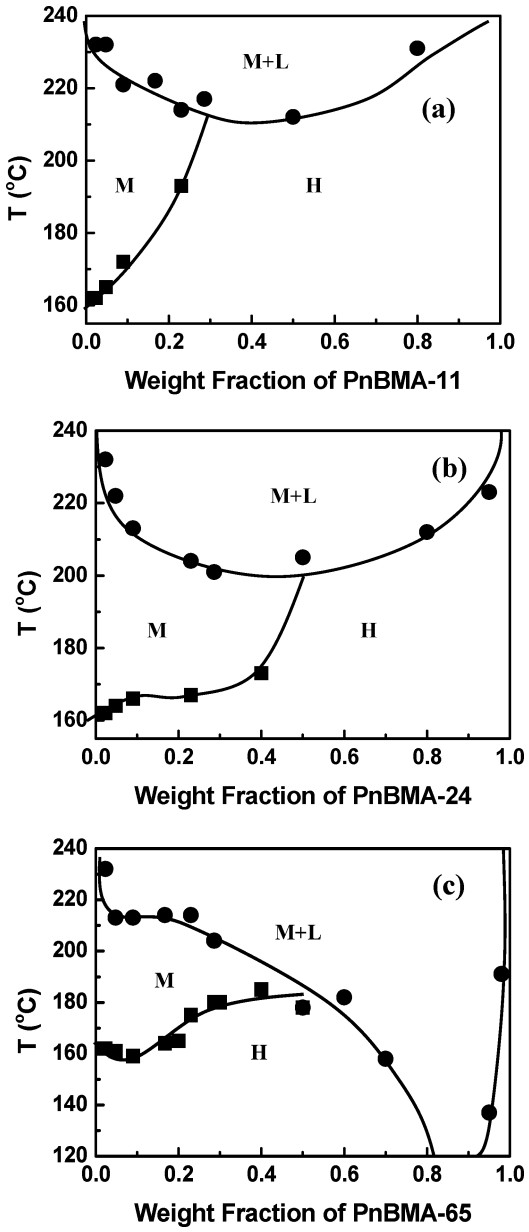

Figure 5. Phase diagrams of mixtures of PS-*b*-PnBMA/PnBMA with three different molecular weights: (a) PnBMA-11; (b) PnBMA-24; (c) PnBMA-65. Here, M, H, and L represent microphase separation, homogeneous state, and macrophase-separated homopolymer, respectively.

fact that ill-defined microdomain structure as shown in Figure 8c was found for PS-*b*-PnBMA/PnBMA-65 mixture but not observed for PS-*b*-PnBMA/PS-68 mixture, might be due to the asymmetric phase behavior nature of neat PS-*b*-PnBMA.[38] As w_{PS} (or w_{PnBMA}) increased further (for instance, 20/80(w/w) PS-*b*-PnBMA/PS-68 and 20/80(w/w) PS-*b*-PnBMA/PnBMA-65), macrophase separation occurred at 190 °C. However, we observed that 20/80(w/w) PS-*b*-PnBMA/PS-68 mixture at 190 °C looked translucent, whereas 20/80(w/w) PS-*b*-PnBMA/PnBMA-65 became very turbid.

Comparing TEM images given in Figure 8 of the mixtures with PS-68 and PnBMA-65, we consider that the effect of PnBMA homopolymer on the phase behavior of the mixtures is quite different from that of PS homopolymer, even though both homopolymers have very similar molecular weight. This suggests that the free volume effect arising from the disparity of the isothermal compressibility (κ) should be an important parameter in determining the phase behavior of a mixture with

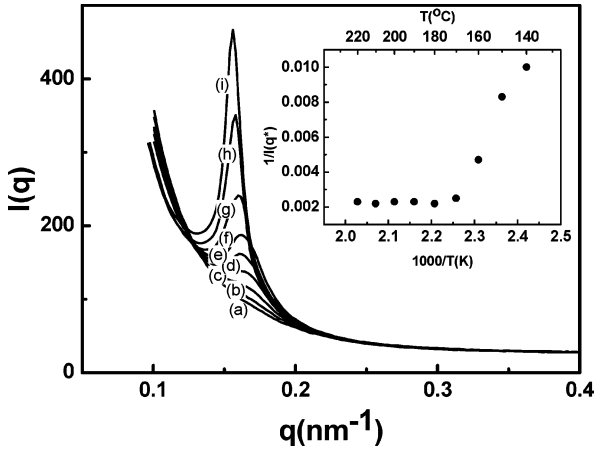

Figure 6. SAXS profiles of 60/40 (w/w) PS-*b*-PnBMA/PS-68 mixture at various temperatures (°C): (a) 140; (b) 150; (c) 160; (d) 170; (e) 180; (f) 190; (g) 200; (h) 210; and (i) 220.

a block copolymer exhibiting LDOT. It is noted that the value of κ (5.1×10^{-5} (1/bar)) at 159.3 °C of PnBMA is larger than that (4.0×10^{-5} (1/bar)) of PS homopolymer.[52]

Figure 9 gives LDOT changes with the amount of PS and PnBMA homopolymers in the mixtures of PS-*b*-PnBMA/PS (Figure 9a) and PS-*b*-PnBMA/PnBMA (Figure 9b) as a function of molecular weight. The LDOT of the mixtures at smaller volume fractions of PS homopolymer (~0.1) increased with increasing amount of PS homopolymer when the molecular weight of PS homopolymer ($M_{H,\,PS}$) was less than 13000. To obtain the volume fraction, the constant specific volumes (in cm^3/g) of PS (0.952) and PnBMA (0.957) were used. Previously, Leibler and Benoit[27] and Noolandi and co-workers[28,29] predicted that when the molecular weight of a homopolymer is less than one-quarter of the total molecular weight of a symmetric block copolymer, the ODT decreases with increasing volume fraction of the homopolymer. Thus, this prediction might be valid for the mixture of a block copolymer with LDOT and a homopolymer, although the transition mechanism of LDOT is quite different from that of ODT. At $M_{H,\,PS}$ greater than 20000, the LDOT decreased initially with increasing amount of PS homopolymer. For the mixtures of PS-*b*-PnBMA/PnBMA, the general trend of the change of LDOT with molecular weight of PnBMA homopolymer is similar to that for the mixtures of PS-*b*-PnBMA/PS. However, at a given amount of the homopolymer, the increase of LDOT of a mixture of PS-*b*-PnBMA/PnBMA is smaller than that of PS-*b*-PnBMA/PS. Specifically, the LDOT of the PS-*b*-PnBMA/PS-13 mixture are always higher than that of the PS-*b*-PnBMA/PnBMA-11 mixture at a given volume fraction of the homopolymer. On the other hand, it is reported that at a given homopolymer volume fraction, the change of ODT for mixtures of a symmetric block copolymer (A-*b*-B) and homopolymer A would be very similar to that for a mixture of A-*b*-B and homopolymer B, as long as the molecular weight of homopolymer A is similar to that of homopolymer B, as a consequence of the incompressible random-phase approximation (RPA) theory.[27−29] We found that the predicted spinodal temperatures based on the incompressible RPA for the PS-*b*-PnBMA/PS-13 mixture are always lower than those for the PS-*b*-PnBMA/PnBMA-11 mixture at a given volume fraction of homopolymer, as demonstrated in the Appendix (see Figure 14). Thus, this result given in Figure 9 again indicates that an additional parameter such as the free volume effect (or disparity of the isothermal compressibility) becomes important in deciding the LDOT.

Now, we compare experimental results with predictions based on a recently developed compressible RPA theory[41−45] in connection with an off-lattice equation-of-state model by Cho and Sanchez.[58] The detailed calculation procedure by the compressible RPA theory is given in the appendix. For the calculation, various molecular parameters should be estimated: the self-interaction parameter ϵ_{ii}, the monomer diameter σ_i, the chain size N_i for pure polymers of molecular weight M_w, and the parameter ϵ_{ij} for cross interaction between different polymers. Certain directional interactions[45] should also be incorporated in the compressible RPA theory to interpret the phase behavior of polystyrene-*block*-poly(*n*-pentyl methacrylate) copolymer, which exhibits immiscibility loop.[53−57] The same approach is performed for neat PS-*b*-PnBMA and binary mixtures with PS or PnBMA, because PS-*b*-PnBMA is expected to have inherently similar directional interaction. The cross-contact interaction parameter ϵ_{ij} is identified as ϵ_{ij}^{ns} without directional interaction but modified by energy increment $\delta\epsilon$ for directional interaction with a Boltzmann counting for such contacts. All of those molecular parameters for the PS/PnBMA system are given in Appendix B-2.

Figure 10 shows plots of predicted spinodal temperatures for the mixture of PS-*b*-PnBMA/PS-68 vs volume fraction of PS-68. Even though mean-field spinodals do not provide information on cloud points or microphase ordered structures, the depression of LDOT at smaller volume fractions of PS-68 is satisfactorily predicted. In addition, the asymmetry in the macrophase separation line toward PS-68 homopolymer is also observed. These two results are harmonious with Figure 4d. Other aspects in this figure, such as phase equilibria, are not considered from the present scattering spinodal calculations. Figure 11 gives changes of spinodal temperature for microphase separation with volume fraction of PS homopolymer as a function of the molecular weight of PS homopolymer. The general trend of spinodal temperature changes depending on the molecular weight of PS is in agreement with Figure 9a, even though the theory gives large decrease in the case of PS-68.

Figure 12 gives changes of the mean-field micro- and macroseparation spinodal temperatures for the mixtures of PS-*b*-PnBMA/PnBMA-65 with volume fraction of PnBMA-65. The depression of spinodal temperature is consistent with the results given in Figure 5c. The changes in spinodal temperature for microphase separation with the addition of PnBMA homopolymers as a function of the molecular weight of PnBMA homopolymer are depicted in Figure 13. Comparing Figure 11 with Figure 13, the predicted spinodal temperature for PS-*b*-PnBMA/PS-13 mixture is always higher than that for PS-*b*-PnBMA/PnBMA-11 mixture at a given volume fraction of the homopolymers, which is consistent with the results given in Figure 9. We consider that the addition of the more compressible PnBMA homopolymer renders the mixture to be more prone to phase separation, because the disparity in equation-of-state properties always hampers miscibility. On the other hand, as we demonstrated in Appendix A, the incompressible RPA theory could not predict this behavior (see Figure 14). Thus, the free volume effect (and/or specific interaction) should be incorporated to predict the phase behavior of a mixture of a block copolymer with an LDOT and a homopolymer. However, the experimentally observed LODT of PS-*b*-PnBMA/PnMA-65 mixture is higher than that of PS-*b*-PnBMA/PS-68 mixture at a given volume fraction of homopolymers, especially when the volume fraction of the homopolymer is larger than ~0.1 (see Figure 9). This is not consistent with the RPA prediction (see

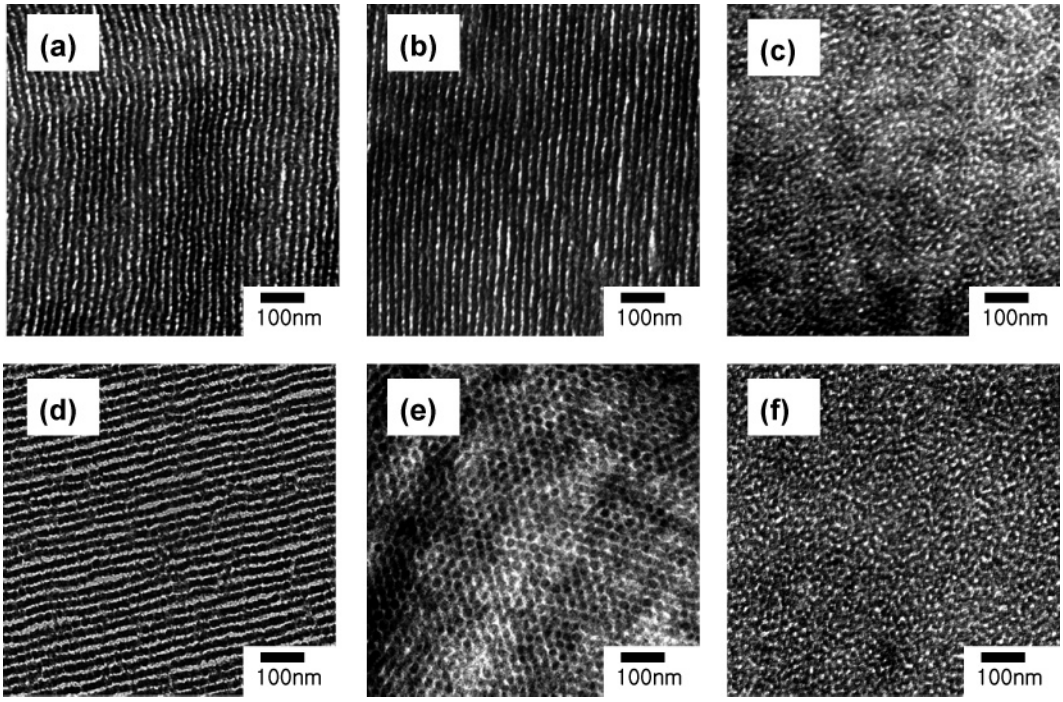

Figure 7. TEM images of (a) neat PS-*b*-PnBMA and various compositions of PS-*b*-PnBMA/PS-20 and PS-*b*-PnBMA/PnBMA-24 mixture. (b) 80/20 and (c) 60/40 (w/w) PS-*b*-PnBMA/PS-20. (d) 80/20, (e) 60/40, and (f) 40/60 (w/w) PS-*b*-PnBMA/PnBMA-24 mixtures. All samples were annealed at 190 °C for 5 days, followed by quenching to room temperature.

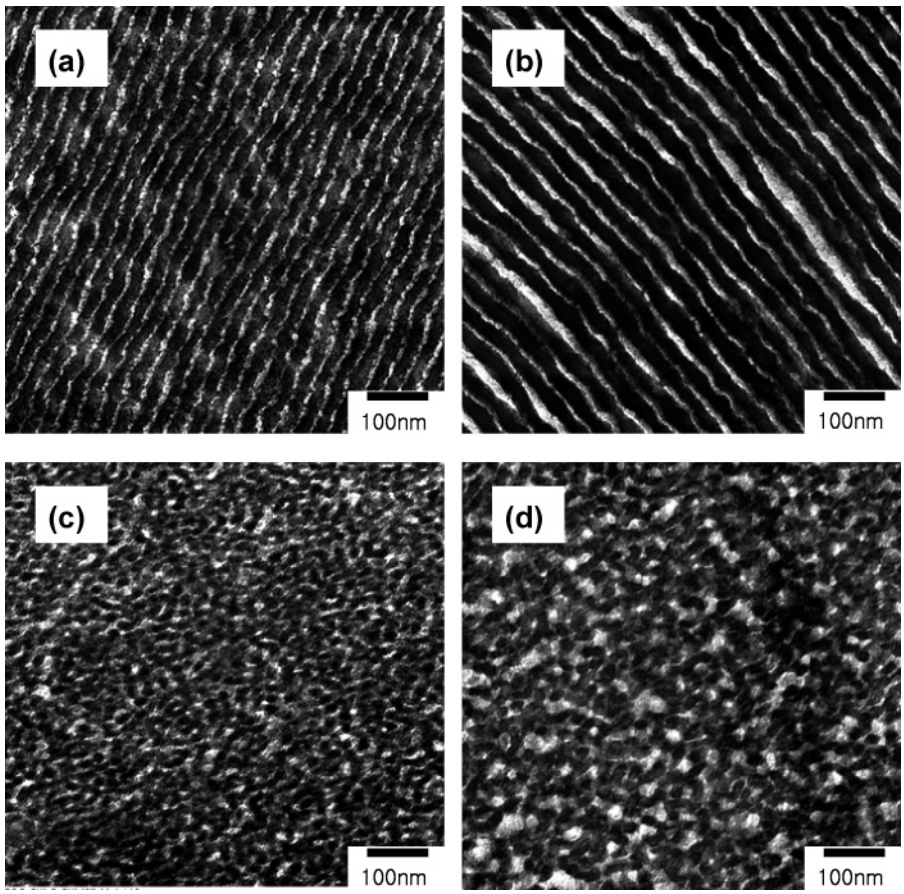

Figure 8. TEM images for various compositions of PS-*b*-PnBMA/PS-68 (a,b) and PS-*b*-PnBMA/PnBMA-65 (c,d) mixtures. (a) 80/20 and (b) 60/40 (w/w) PS-*b*-PnBMA/PS-68; (c) 80/20 and (d) 60/40 (w/w) PS-*b*-PnBMA/PnBMA-65. All samples were annealed at 190 °C for 5 days, followed by quenching to room temperature.

Figures 11 and 13) that the predicted LODT of the former is close to (but at least lower than) that of the latter. We consider that this discrepancy is due to the complex microdomain change for PS-*b*-PnBMA/PnBMA-65 blend. For instance, an ill-defined microdomain was only observed in PnBMA system. Thus, the spinodal temperature predicted by the compressible RPA would not predict accurately such microdomain phase boundary when the molecular weight of PnBMA increases.

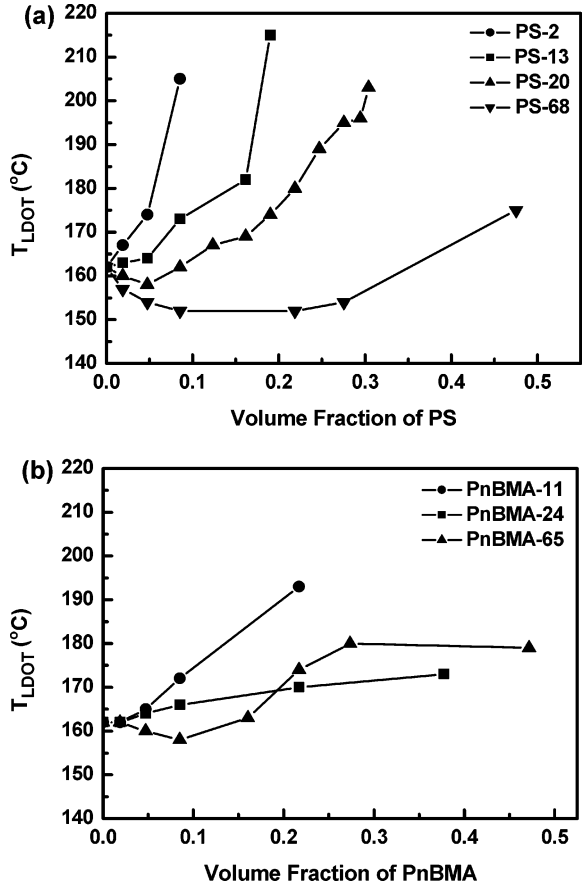

Figure 9. Change of (a) LDOT for PS−PnBMA/PS mixtures with amount of PS homopolymer and (b) LDOT for PS−PnBMA/PnBMA mixtures with amount of PnBMA homopolymer.

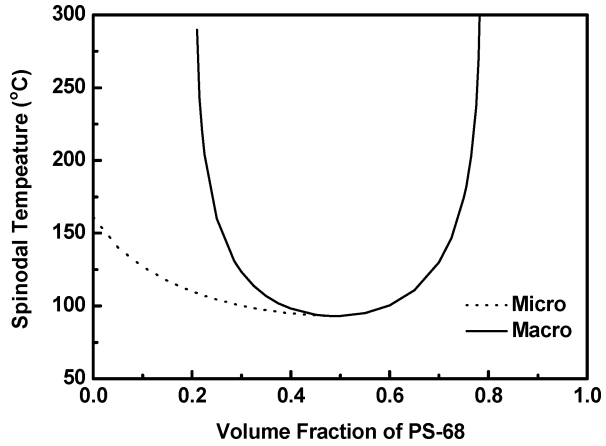

Figure 10. Plots of mean-field spinodal temperatures for microphase (dotted curve) and macrophase (solid curve) separations for the mixture of PS−PnBMA and PS-68 vs the volume fraction of PS-68.

Finally, it is noted that the phase behavior of the mixture of a block copolymer with LDOT and a homopolymer estimated by the mean-field scattering spinodals should be carefully interpreted. A more elaborate Landau analysis with the inclusion of observed microdomains is needed to explain the complete phase behavior of the mixture. Furthermore, the concentration fluctuation effects and micellization need to be taken into the consideration. Concentration fluctuation would be more prominent for A-*b*-B copolymer compared with A/B blend. The addition of shorter homopolymers enhances the fluctuation effect. Also, for a region without microphase separation, the

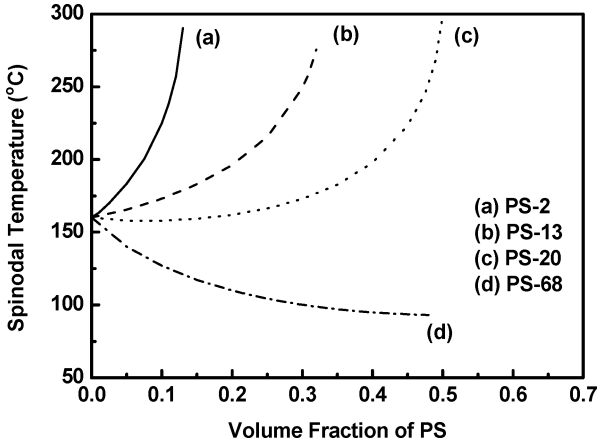

Figure 11. Plots of the mean-field spinodal temperatures for microphase separation for the mixture of PS-*b*-PnBMA and PS vs volume fraction of PS homopolymer as a function of the molecular weight of PS homopolymer.

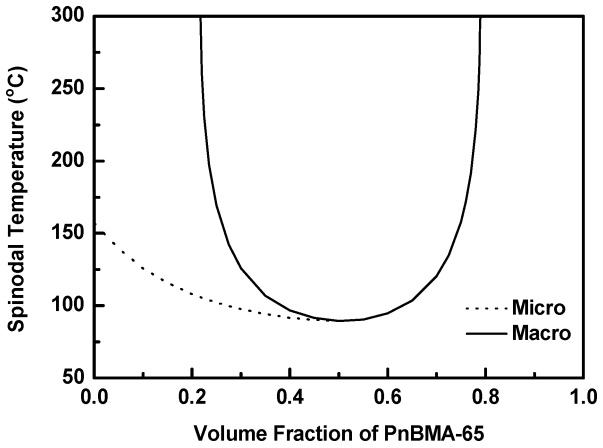

Figure 12. Plots of mean-field spinodal temperatures for microphase (dotted curve) and macrophase (solid curve) separations for the mixture of PS−PnBMA and PnBMA-65 vs the volume fraction of PnBMA-65.

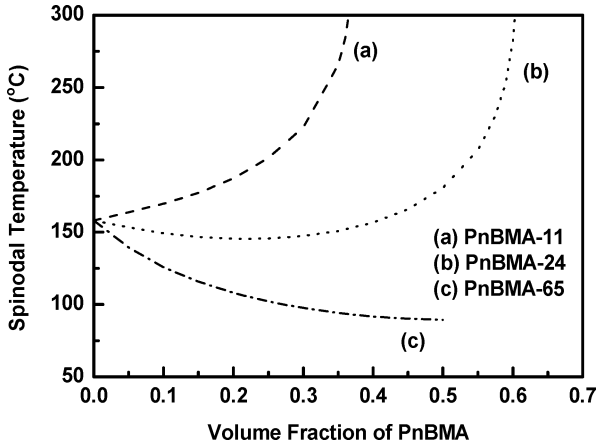

Figure 13. Plots of the mean-field spinodal temperatures for microphase separation for the mixture of PS-*b*-PnBMA and PnBMA vs volume fraction of PnBMA homopolymer as a function of the molecular weight of PnBMA homopolymer.

local concentration fluctuations could induce micellization or microemulsions. This will deserve a future investigation. Nonetheless, the mean-field spinodal analysis is still of great value in exploring the qualitative or semiquantitative phase behavior of the mixture of a block copolymer with LDOT and a homopolymer.

CDV

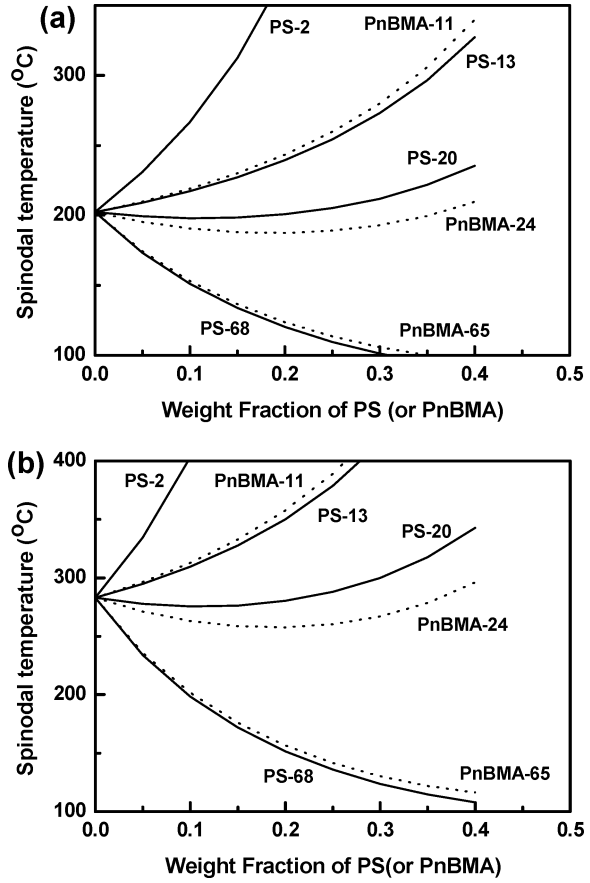

Figure 14. Predicted spinodal temperatures for PS-*b*-PnBMA/PS (solid curves) and PS-*b*-PnBMA/PnBMA (dotted curves) mixtures by using two different expressions of χ: (a) from eq A5; (b) from eq A6.

4. Conclusion

We studied phase behaviors of PS-*b*-PnBMA/PS mixture and PS-*b*-PnBMA/PnBMA mixture depending upon molecular weight of homopolymer. We found that when the molecular weight of a homopolymer is smaller than half of the corresponding block, LDOT increases (thus miscibility is enhanced). This is consistent with the phase behavior found for a mixture of a block copolymer with ODT. However, the changes of microdomains for the PS-*b*-PnBMA/PS mixture are different from those of a PS-*b*-PnBMA/PnBMA mixture, when the molecular weight of homopolymer is large. Namely, for the PS-*b*-PnBMA/PnBMA-65 mixture, lamellar microdomain structure was destroyed with the addition of 20 wt % of PnBMA homopolymer. On the other hand, for the PS-*b*-PnBMA/PS-68 mixture, lamellar microdomain structure was maintained for up to 40% of PS homopolymer. It was shown that the qualitative aspects in the experimental phase behavior of the copolymer mixtures are in agreement with the compressible RPA predictions. But, this phase behavior was not predicted by the incompressible RPA.

Acknowledgment. This work was supported by the National Creative Research Initiative Program supported by the Korea Science and Engineering Foundation (KOSEF). J. C. acknowledges the Hyperstructured Organic Materials Research Center funded by KOSEF. Synchrotron small-angle X-ray scattering was performed at PLS beamlines (4C1 and 4C2) supported by POSCO and KOSEF.

Appendix A. Prediction of the Spinodal Temperature by the Incompressible RPA for a Binary Mixture of an A-*b*-B Copolymer and a Homopolymer A (or B).

According to the incompressible RPA, the structure factor ($\tilde{S}(q)$) of an A-*b*-B copolymer and homopolymer A and B is given by[27−29,59−61]

$$\tilde{S}(q) = 1/\left[\frac{S(q)}{W(q)} - 2\chi\right] \tag{A1}$$

$$S(q) = S_{AA}(q) + 2S_{AB}(q) + S_{BB}(q) \tag{A2a}$$

$$W(q) = S_{AA}(q)\, S_{BB}(q) - (S_{AB}(q))^2 \tag{A2b}$$

in which $S_{ij}(q)$ is given by

$$S_{AA}(q) = \phi_C N_C d(f,N_C) + \phi_{HA} N_{HA} d(1,N_{HA}) \tag{A3a}$$

$$S_{AB}(q) = \phi_C N_C [d(1,N_C) - d(f,N_C) - d(1-f,N_C)]/2 \tag{A3b}$$

$$S_{BB}(q) = \phi_C N_C d(1-f,N_C) + \phi_{HB} N_{HB} d(1,N_{HB}) \tag{A3c}$$

where ϕ_C, ϕ_{HA}, and ϕ_{HB} are the volume fractions of A-*b*-B, homopolymers A and B, respectively; N_C, N_{HA}, and N_{HB} are the degrees of polymerization (or numbers of statistical segments) for A-*b*-B, homopolymers A and B, respectively; and f is the volume fraction of component A in the A-*b*-B. Also, $d(f,N_i)$ is given by

$$d(f,N_i) = 2[fx_i + \exp(-fx_i) - 1]/x_i^2 \tag{A4a}$$

$$x_i = N_i q^2 a_i^2/6 \tag{A4b}$$

Here, a_i is the statistical segment length of component i (= C, HA, and HB).

Two expressions of the Flory segmental interaction (χ) for PS-*b*-PnBMA are available in the literature:[35b,37]

$$\chi = 0.028 - 5.8/T \quad \text{from ref 35b} \tag{A5}$$

$$\chi = 0.024 - 4.56/T \quad \text{from ref 37} \tag{A6}$$

The spinodal temperatures of microphase-separation of the mixture of an A-*b*-B and homopolymers A and B are obtained from $1/\tilde{S}(q^*) \rightarrow 0$, in which q^* is the positive value at which $S(q)/W(q)$ becomes the minimum.

Parts a and b of Figure 14 are the spinodal temperatures for PS-*b*-PnBMA/PS and PS-*b*-PnBMA/PnBMA mixtures calculated from eqs A5 and A6, respectively. It is noted that even though the *x*-axis is changed into volume fraction of each homopolymer, the predicted LDOT is essentially the same due to similar values of the specific volume of PS (0.952 cm^3/g) and PnBMA(0.957 cm^3/g). It seems that the predicted phase behavior is consistent with the results given in Figure 9, parts a and b, although the predicted LODT of neat PS-*b*-PnBMA is higher than the measured one. However, when we compare the predicted spinodal temperatures for PS-*b*-PnBMA/PS-13 mixture and PS-*b*-PnBMA/PnBMA-11 mixture, the prediction is opposite to the experimental results. Namely, the predicted spinodal temperatures for the PS-*b*-PnBMA/PS-13 mixture are always lower than those for the PS-*b*-PnBMA/PnBMA-11 mixture at a given volume fraction of homopolymer, even though the difference is small. On the other hand, the measured LDOT for the former was always higher than those for the latter. Thus, we consider that incompressible RPA theory could not predict

correctly the phase diagram for the mixture consisting of a block copolymer with LDOT and a homopolymer.

Appendix B. Derivation of the Compressible RPA for a Binary Mixture of an A-*b*-B Copolymer and a Homopolymer A (or B)

B-1. Compressible RPA. An RPA is an approximation method to calculate the second-order monomer−monomer correlation function $G_{ij}^{(2)}$, or equivalently S_{ij}, and higher-order correlation functions $G^{(n)}$'s for the analysis of phase segregation in polymer blends and block copolymers.[62,63] Recently, one of us successfully combined the RPA with the Cho-Sanchez (CS) equation-of-state model to analyze compressibility effects.[41−45,58,64−65]

We consider the mixture of an A-*b*-B copolymer of size N with a close-packed (hard-core) volume fraction ϕ_b and a homopolymer A of size y_hN with a close-packed volume fraction ϕ_h. On each copolymer chain, f_i indicates a close-packed volume fraction for i-block, and N_i each block size as $N_i = f_i N$. Phase segregation in the system is characterized by proper order parameters. A natural choice of order parameters can be given as the thermal average of the difference between local density $\eta_i(\vec{r})$ and global density η_i of i-constituent as $\psi_i \equiv \langle \eta_i(\vec{r}) - \eta_i \rangle$. The η_A and η_B are, respectively, related to the overall density η as $\eta_A = (\phi_h + \phi_b f_A)\eta$ and $\eta_B = \phi_b f_B \eta$. The Landau expansion of the free energy is expressed as a series in the order parameter ψ_i, where the coefficients in the Landau expansion are called the vertex functions $\Gamma^{(n)}$. The ψ_i can also be expanded as a series in U_i, which is conjugate to the order parameter ψ_i. The coefficients appearing in the series for ψ_i are the correlation functions $G^{(n)}$'s. In estimating ψ_i, the correlation functions $G^{(n)}$ are supposed to be equal to those of noninteracting Gaussian copolymer chains, which are denoted as $G^{(n)0}$. The external potential U_i is then substituted with U_i^{eff}, which is corrected as $U_i^{\text{eff}} = U_i + W_{ij}\psi_j$ to properly take the interaction effects into account by an interaction field W_{ij}.[42,58] The W_{ij} is formulated from the CS model to include the desired compressibility effects, and thus includes attractive i,j interactions and excluded volume interactions. The resultant self-consistent field equation is solved by an iterative technique to obtain correlation functions. The correlation functions then yield the vertex functions. The second-order vertex function is related to energetic terms as[41−45,58,64−65]

$$\Gamma_{ij}^{(2)} = 1/S_{ij} = 1/S_{ij}^{\,0} + W_{ij}/kT \tag{B1}$$

where k is the Boltzmann's constant, T is the absolute temperature, and $S_{ij}^{\,0}$ is the Gaussian correlation function for the mixture of an A-*b*-B copolymers with homopolymer A as

$$\eta S_{ij}^{\,0} = \phi_b N \delta_{ij}[\delta_{iA} d(x,f_A) + \delta_{jB} d(x,f_B)] + \phi_b N \delta_{iA}\delta_{jB} g(x,f_A) g(x,f_B) + \phi_h N y_h \delta_{ij}\delta_{iA} d(y_h x, f_A) \tag{B2}$$

The two functions, $d(x,f_i)$ and $g(x,f_i)$, are given as $d(x,f_i) = 2(f_i x + e^{-f_i x} - 1)/x^2$ and $g(x,f_i) = (1 - e^{-f_i x})/x$, respectively, where x $(=q^2 R_g^2)$ implies the dimensionless square of wave number with the gyration radius R_g of the copolymer. The symbol δ_{ij} indicates the Kronecker δ. The overall density η in the Gaussian functions corrects the diluted contact probabilities by the presence of free volume. The third or higher-order vertex functions are purely entropic and not involved in energetics.

The CS free energy is given as $F_0 = F_0^{id} + F_0^{EV} + U^{nb}$. The F_0^{id} represents the ideal free energy of the noninteracting Gaussian chain system. The F_0^{EV} and U^{nb} stand for the contribution to the free energy from the excluded volume effects and the attractive interactions between nonbonded monomers, respectively. The W_{ij} is formulated as the second-order derivative of the nonideal part of the CS free energy per system volume V with respect to η_i's as[41−45,58,64−65]

$$\beta W_{ij}/v^* = \partial^2[(\beta F_0^{\,EV} + \beta U^{nb})/V]/\partial\eta_i \partial\eta_j \tag{B3}$$

where $\beta = 1/kT$ and v^* $(= \pi\sigma^3/6)$ implies the volume of monomers having a diameter σ. The contributions from F_0^{EV} and U^{nb} in eq B3 are, respectively, denoted as L_{ij}/v^* and $[-\beta\epsilon_{ij}^{\text{app}}]/v^*$, where these two in the high molecular weight limit are properly written as follows:

$$L_{ij}(\eta) = \frac{3}{2}\left[\frac{4}{(1-\eta)^3} + \frac{6\eta}{(1-\eta)^4} - \frac{2}{(1-\eta)^2} - \frac{2\eta}{(1-\eta)^3}\right] \tag{B4}$$

and

$$-\beta\epsilon_{ij}^{\text{app}}(\eta) = \beta h_z \epsilon_{ij} f_p \frac{u(\eta)}{\eta} + \beta\Big(\sum_k \eta_k\{h_z\epsilon_{ik} + h_z\epsilon_{jk}\} f_p \frac{\partial}{\partial\eta}\left(\frac{u(\eta)}{\eta}\right) + \frac{1}{2}\beta\Big(\sum_{kl}\eta_k\eta_l h_z\epsilon_{kl}\Big) f_p \frac{\partial^2}{\partial\eta^2}\left(\frac{u(\eta)}{\eta}\right) \tag{B5}$$

In eq B5, $h_z\epsilon_{ij}$ denotes the characteristic i,j-interaction parameter and $u(\eta) = (\gamma/C)^4\eta^4 - (\gamma/C)^2\eta^2$, with $\gamma = 1/\sqrt{2}$ and $C = \pi/6$, describes the density dependence of attractive nonbonded interactions. The numeric prefactor f_p associated with $u(\eta)$ is simply $f_p = 4$.

In many cases, it is more convenient to use the order parameters $\bar{\psi}_1$ $(\equiv \langle \eta_A(\vec{r}) - \eta_A\rangle/2\eta - \langle \eta_B(\vec{r}) - \eta_B\rangle/2\eta)$ and $\bar{\psi}_2$ $(=\psi_A + \psi_B)$ instead of the original ψ_i. Here, $\bar{\psi}_1$ represents the fluctuations in either A or B density, and $-\bar{\psi}_2$ the fluctuations in free volume fraction. The vertex function $\Gamma^{(n)}$ in the Landau expansion of the free energy in ψ_i is then replaced with the proper vertex function $\bar{\Gamma}^{(n)}$. It should be noted that the subscripts in $\bar{\Gamma}^{(n)}$ take 1 and 2, which, respectively, indicate $\bar{\psi}_1$ and $\bar{\psi}_2$, not the constituents. The second-order vertex functions $\bar{\Gamma}^{(2)}$'s are only written here as[42−45,64−65]

$$[\bar{\Gamma}_{ij}^{\,(2)}] = \begin{bmatrix} \eta^2(\Gamma_{11}^{\,(2)} - 2\Gamma_{12}^{\,(2)} + \Gamma_{22}^{\,(2)}) & \eta/2\cdot(\Gamma_{11}^{\,(2)} - \Gamma_{22}^{\,(2)}) \\ \eta/2\cdot(\Gamma_{11}^{\,(2)} - \Gamma_{22}^{\,(2)}) & \Gamma_{11}^{\,(2)}/4 + \Gamma_{12}^{\,(2)}/2 + \Gamma_{22}^{\,(2)}/4 \end{bmatrix} \tag{B6}$$

It was shown that $\bar{\Gamma}_{12}^{(2)} \propto (\epsilon_{AA} - \epsilon_{BB})$ for a symmetric diblock copolymer. Even for asymmetric copolymers, $\bar{\Gamma}_{12}^{(2)}$ is dominated by the term with $(\epsilon_{AA} - \epsilon_{BB})$, as $1/S_{ij}^{\,0} \sim O(1/N)$ and $L_{AA} \approx L_{BB}$ for high polymers. Therefore, $\bar{\Gamma}_{12}^{(2)}$ signifies the disparity in equation-of-state properties between the constituents A and B.[43−45]

Meanwhile, the equilibrium overall density η is determined at a given set of temperature and pressure from the following CS equation of state for high polymers:[41,58]

$$\beta P = \frac{1}{v^*}\left[\frac{3}{2}\frac{(\eta^2 + \eta^3)}{(1-\eta)^3}\right] + \frac{f_p}{2}\frac{\beta h_z\epsilon}{v^*}[4(\gamma/C)^4\eta^5 - 2(\gamma/C)^2\eta^3] \tag{B7}$$

where $h_z\epsilon$ implies the average interaction parameter for the given mixture system.

Finally, the spinodals are estimated through the condition of $\det[S^{-1}] = 0$ (or $\det[S] \to \infty$), since scattering experiment can

be considered as a μVT ensemble. Microphase separation is characterized by this condition with finite scattering vector $q^* > 0$, while macrophase separation is signified by $q^* = 0$.

B-2. Molecular Parameters for PS/PnBMA in the Compressible RPA Approach. To characterize a given block copolymer system by the compressible RPA theory,[45] various molecular parameters should be estimated: the self-interaction parameter ϵ_{ii}, the monomer diameter σ_i, the chain size N_i for pure polymers, and the parameter ϵ_{ij} for cross interaction between different polymers. Those parameters for PS (1) and PnBMA (2) are estimated as follows.[66] $\sigma_1 = \sigma_2 = 4.04$ Å, $h_z\epsilon_{11}/k = 4107.0$ K, $h_z\epsilon_{22}/k = 3738.2$ K, $N_1\pi\sigma_1^3/6M_w = 0.41857$ cm^3/g, $N_2\pi\sigma_2^3/6M_w = 0.42042$ cm^3/g. Here, h_z is the number of nonbonded nearest neighbors surrounding a chosen monomer, and $h_z \approx 10$ for dense polymeric liquids. It is seen that PnBMA is more compressible than PS ($\epsilon_{22} < \epsilon_{11}$), which is also consistent with the fact that the isothermal compressibility (5.1×10^{-5} (1/bar)) at 159.3 °C of PnBMA is larger than that (4.0×10^{-5} (1/bar)) of PS homopolymer.[52]

The directional interaction in the PS/PnBMA system is incorporated in the following way. The central concept is to take the 1, 2 cross-contact interaction parameter ϵ_{12} as a kind of free energy that possesses not only enthalpic but also entropic contributions. Consider that the cross-contact interaction can be nonspecific with a characteristic energy parameter ϵ_{12}^{ns} and specific with the energy parameter $\epsilon_{12}^{ns} + \delta\epsilon$. The fraction θ of the total number of cross-contacts that are specific is given from Boltzmann statistics as $\theta = [1 + d\exp(-\delta\epsilon/kT)]^{-1}$, where the symbol d denotes the ratio of the statistical degeneracies of nonspecific and specific cross-contact interactions. The ϵ_{12} per one cross-contact can then be suggested as $\epsilon_{12} = \epsilon_{12}^{ns} + \delta\epsilon - kT\ln[\theta(1+d)]$. Here, the degeneracy ratio d is not taken as an adjustable parameter, but fixed to 11, which implies the direction interaction pair is formed only in the limited range of spatial arrangement of two dissimilar monomers. Finally, to fit the measured LDOT (160 °C) for neat PS-*b*-PnBMA with molecular weight of 67000, the remaining parameters, ϵ_{12}^{ns} and $\delta\epsilon/k$, are adjusted as $0.98363(\epsilon_{11}\epsilon_{22})^{1/2}$ and 74 K, respectively.[68]

References and Notes

(1) Kinning, D. J.; Winey, K. I.; Thomas, E. L. *Macromolecules* **1988**, *21*, 3502.
(2) Kinning, D. J.; Thomas, E. L.; Fetters, L. J. *J. Chem. Phys.* **1988**, *90*, 5806.
(3) Winey, K. I.; Thomas, E. L.; Fetters, L. J. *J. Chem. Phys.* **1991**, *95*, 9367; *Macromolecules*, **1992**, *25*, 422 and 2645.
(4) Hashimoto, T.; Tanaka, H.; Hasegawa, H. *Macromolecules* **1990**, *23*, 4378.
(5) Tanaka, H.; Hashimoto, T. *Macromolecules* **1991**, *24*, 5713.
(6) Tanaka, H.; Hasegawa, H.; Hashimoto, T. *Macromolecules* **1991**, *24*, 240.
(7) Koizumi, S.; Hasegawa, H.; Hashimoto, T. *Macromol. Chem. Macromol. Symp.* **1992**, *62*, 75.
(8) Hashimoto, T.; Koizumi, S.; Hasegawa, H.; Izumitani, T.; Hyde, S. T. *Macromolecules* **1992**, *25*, 1433.
(9) Hashimoto, T.; Yamasaki, K.; Koizumi, S.; Hasegawa, H. *Macromolecules* **1993**, *26*, 2895.
(10) Koizumi, S.; Hasegawa, H.; Hashimoto, T. *Macromolecules* **1994**, *27*, 6532.
(11) Koizumi, S.; Hasegawa, H.; Hashimoto, T. *Macromolecules* **1994**, *27*, 7893.
(12) Zin, W. C.; Roe, R. J. *Macromolecules* **1984**, *17*, 183.
(13) Roe, R. J.; Zin, W. C. *Macromolecules* **1984**, *17*, 189.
(14) Rigby, D.; Roe, R. J. *Macromolecules* **1984**, *17*, 1778.
(15) Rigby, D.; Lin, J. L.; Roe, R. J. *Macromolecules* **1985**, *18*, 2269.
(16) Rigby, D.; Roe, R. J. *Macromolecules* **1986**, *19*, 721.
(17) Roe, R. J. *Macromolecules* **1986**, *19*, 728.
(18) Nojima, S.; Roe, R. J. *Macromolecules* **1987**, *20*, 1866.
(19) Disko, M. M.; Liang, K. S.; Behal, S. K.; Roe, R. J.; Jeon, K. J. *Macromolecules* **1993**, *26*, 2983.
(20) Jeon, K. J.; Roe, R. J. *Macromolecules* **1994**, *27*, 2439.
(21) Kang, C. K.; Zin, W. C. *Macromolecules* **1992**, *25*, 3039.
(22) Spontak, R. J.; Smith, S. D.; Ashraf, A. *Macromolecules* **1993**, *26*, 956.
(23) Spontak, R. J.; Smith, S. D.; Ashraf, A. *Macromolecules* **1993**, *26*, 5118.
(24) Han, C. D.; Baek, D. M.; Kim, J.; Kimishima, K.; Hashimoto, T. *Macromolecules* **1992**, *25*, 3052.
(25) Baek, D. M.; Han, C. D.; Kim, J. K. *Polymer* **1992**, *33*, 4821.
(26) Lõwenhaupt, B.; Steurer, A.; Hellmann, G. P.; Gallot, Y. *Macromolecules* **1994**, *27*, 908.
(27) Leibler, L.; Benoit, H. *Polymer* **1981**, *2*, 195.
(28) Hong, K. M.; Noolandi, J. *Macromolecules* **1983**, *16*, 1083.
(29) Whitmore, M. D.; Noolandi, J. *Macromolecules* **1985**, *18*, 2486.
(30) Banaszak, M.; Whitmore, M. D. *Macromolecules* **1992**, *25*, 2757.
(31) Matsen, M. W. *Macromolecules* **1995**, *28*, 5765.
(32) Janert, P. K.; Schick, M. *Macromolecules* **1998**, *31*, 1109.
(33) Russell, T. P.; Karis, T. E.; Gallot, Y.; Mayes, A. M. *Nature (London)* **1994**, *368*, 729.
(34) Russell, T. P.; Karis, T. E.; Gallot, Y.; Mayes, A. M. *Macromolecules* **1995**, *28*, 1129.
(35) (a) Pollard, M.; Ruzette, A. V.; Mayes, A. M.; Gallot, Y.; Russell, T. P. *Macromolecules* **1998**, *31*, 6493. (b) Ruzette, A. V. G.; Mayes, A. M.; Pollard, M.; Russell, T. P.; Hammouda, B. *Macromolecules* **2003**, *36*, 3351.
(36) Hasegawa, H.; Sakamoto, N.; Takeno, H.; Jinnai, H.; Hashimoto, T.; Schwahn, D.; Frielinghaus, H.; Janben, S.; Imai, M.; Mortensen, K. *J. Phys. Chem. Solids* **1999**, *60*, 1307.
(37) Weidisch, R.; Stamm, M.; Schubert, D. W.; Arnold, M.; Budde, H.; Horing, S. *Macromolecules* **1999**, *32*, 3405.
(38) Fischer, H.; Weidisch, R.; Stamm, M.; Budde, H.; Horing, S. *Colloid Polym. Sci.* **2000**, *278*, 1019.
(39) Jeong, U.; Ryu, D. Y.; Kim, J. K. *Macromolecules* **2003**, *36*, 8913. Li, C.; Lee, D. H.; Kim, J. K.; Ryu, D. Y.; Russell, T. P. *Macromolecules* **2006**, *39*, 5926.
(40) Sanchez, I. C. In *Polymer Compatibility and Incompatibility*, Solc, K., Ed.; MMI Press: New York, 1982.
(41) Cho, J. *Macromolecules* **2000**, *33*, 2228.
(42) Cho, J. *Macromolecules* **2001**, *34*, 1001.
(43) Cho, J. *J. Chem. Phys.* **2003**, *119*, 5711.
(44) Cho, J. *J. Chem. Phys.* **2004**, *120*, 9831.
(45) Cho, J. *Macromolecules* **2004**, *37*, 10101.
(46) Balsara, N. P.; Perahia, D.; Safinya, C. R.; Tirrell, M.; Lodge, T. P. *Macromolecules* **1992**, *25*, 3896. Balsara, N. P.; Dai; H. J.; Kesani, P. K.; Garetz, B. A.; Hammouda, B. *Macromolecules* **1994**, *27*, 7406.
(47) Bolze, J.; Kim, J.; Huang, J. Y.; Rah, S.; Youn, H. S.; Lee, B.; Shin, T. J.; Ree, M. *Macromol. Res.* **2002**, *10*, 2.
(48) Rosedale, J. H.; Bates, F. S. *Macromolecules* **1990**, *23*, 2329.
(49) Bates, F. S.; Rosedale, J. H.; Fredrickson, G. H. *J. Chem. Phys.* **1990**, *92*, 6255.
(50) Han, C. D.; Baek, D. M.; Kim, J. K. *Macromolecules* **1990**, *23*, 561. Han, C. D.; Baek, D. M.; Kim, J. K.; Ogawa, T.; Hashimoto. T. *Macromolecules* **1995**, *28*, 5043.
(51) Sagamoto, N.; Hashimoto, T. *Macromolecules* **1998**, *31*, 3815, 8493.
(52) Zoller, P.; Walsh, D. J. *Standard Pressure−Volume−Temperature Data for Polymers*; Technomic Pub.: Lancaster, PA, 1995; pp 25, 135, 161.
(53) Ryu, D. Y.; Jeong, U.; Kim, J. K.; Russell, T. P. *Nat. Mater.* **2002**, *1*, 114. Ryu, D. Y.; Jeong, U. Lee, D. H.; Kim, J.; Youn, H. S.; Kim, J. K. *Macromolecules* **2003**, *36*, 2894.
(54) Ryu, D. Y.; Lee, D. J.; Kim, J. K.; Lavery, K. A.; Russell, T. P.; Han, Y. S.; Seong, B. S.; Lee, C. H.; Thiyagarajan, P. *Phys. Rev. Lett.* **2003**, *90*, 235501.
(55) Ryu, D. Y.; Lee, D. H.; Jeong, U.; Yun, S. H.; Park, S.; Kwon, K.; Sohn, B. H.; Chang, T.; Kim, J. K.; Russell, T. P. *Macromolecules* **2004**, *37*, 3717. Ryu, D. Y.; Lee, D. H.; Jang, J. Kim, J. K.; Lavery, K. A.; Russell, T. P. *Macromolecules* **2004**, *37*, 5851.
(56) Kim, J. K.; Jang, J.; Lee, D. H.; Ryu, D. Y. *Macromolecules* **2004**, *37*, 8599.
(57) Kim, H. J.; Kim, S. B.; Kim, J. K.; Jung, Y. M.; Ryu, D. Y.; Lavery, K. A.; Russell, T. *Macromolecules* **2006**, *39*, 408.
(58) Cho, J.; Sanchez, I. C. *Macromolecules* **1998**, *31*, 6650.
(59) Mori, K.; Tanaka, H.; Hashimoto, T. *Macromolecules* **1987**, *20*, 381.
(60) Kim, J. K.; Kimishima, K.; Hashimoto, T. *Macromolecules* **1993**, *26*, 125.
(61) Kim, J. K. *Polymer* **1995**, *36*, 1243.
(62) de Gennes, P.-G. *Scaling Concepts in Polymer Physics*; Cornell University Press: Ithaca, NY, 1979.
(63) Leibler, L. *Macromolecules* **1980**, *13*, 1602.
(64) Cho, J. *Macromolecules* **2001**, *34*, 6097.
(65) Cho, J. *Macromolecules* **2002**, *35*, 5697.

(66) Three molecular parameters for PS were determined by best fit of the volume data of PS given in ref 67 by using the Cho-Sanchez equation-of-state model.[58] We found that the errors associated with the fitting for σ_1, ϵ_{11}, and $N_1\sigma_1^3/M_w$ are 0.5, 0, and 0.1%, respectively. The monomer diameter (σ_2) of PnBMA was set to be equal to that of PS, and the other two parameters of PnBMA were determined by best fit of the volume data of PnBMA in ref 52 to satisfy the condition of the identical monomer sizes. The estimation errors for ϵ_{22} and $N_2\sigma_2^3/M_w$ are 2.0 and 0.2%, respectively.

(67) Quach, A.; Simha, R. *J. Appl. Phys.* **1971**, *42*, 4592.

(68) These two (ϵ_{12}^{ns} and $\delta\epsilon/k$) are the only adjustable parameters for describing the phase behavior in this work. Adjusting these can in principle give a precise fit of measured LDOT data. We found that the predicted LDOT was changed by ± 4 K when $\epsilon_{12}^{ns}/(\epsilon_{11}\epsilon_{22})^{1/2}$ is changed by ∓ 0.00024 and $\delta\epsilon/k$ by ± 1. It is noted that the experimental error measured by SAXS and birefreingence is within ± 2 K.

MA0617567